Research Square

Preprints are preliminary reports that have not undergone peer review.
They should not be considered conclusive, used to inform clinical practice,
or referenced by the media as validated information.

Site selection from space for urban design: aligning EO surface thermal patterns with urban form and functions

Gabriele Oneto

gabriele.oneto@edu.unige.it

University of Genoa

Luca Cenci

CIMA Research Foundation

Filippo Fraschini

CIMA Research Foundation

Luca Pulvirenti

CIMA Research Foundation

Katia Perini

University of Genoa

Research Article

Keywords: Data-driven urban planning, surface urban heat island, morphometrics, spatial analysis, remote sensing, multicriteria assessment

Posted Date: September 16th, 2026

DOI: https://doi.org/10.21203/rs.3.rs-9115415/v1

License: This work is licensed under a Creative Commons Attribution 4.0 International License.
Read Full License

Additional Declarations: No competing interests reported.

Title. Site selection from space for urban design: aligning EO surface thermal patterns with urban form and functions.

Abstract.

Earth observations enable consistent and spatially contiguous city-wide observations, yet their effective integration into urban planning remains a challenge. Surface thermal patterns reflect the interplay between urban forms (morphology, density) and functions (land use, sociodemographic vulnerability), but most assessment methods rely on spatial units that are not aligned with how architects and planners understand and transform urban space. This limits their usefulness for design practice, which works through plots and blocks that reflect spatial form but overlook functional conditions essential to understanding heat vulnerability. We present a method that integrates forms and functions to support site selection, using a multicriteria ranking based on more than fifty variables capturing exposure, vulnerability, and hazard conditions from satellite data, and a site characterization approach that groups areas with similar form- and function-related attributes. The workflow integrates morphogenetic spatial modules, multicriteria decision making, and clustering, and is tested in Genoa and Turin to examine how different combinations of spatial units, algorithms, and weighting schemes influence the results. Although the results are based on earth observation data, the methodology can be easily adapted to different data sources on hazards to assess the form and function inferences.

Keywords. Data-driven urban planning; surface urban heat island; morphometrics; spatial analysis; remote sensing; multicriteria assessment.

1. List of abbreviations

AOI - Area of Interest

CB - Census Blocks

CEST - Central European Summer Time

EO - Earth Observation

ET - Enclosed Tessellation

GHS-FUA - Global Human Settlement – Functional Urban Area

HAC - Hierarchical Agglomerative Clustering

IPCC – Intergovernmental Panel on Climate Change

LCZ - Local Climate Zone

LST - Land Surface Temperature

MAUP - Modifiable Areal Unit Problem

MCDM - Multicriteria Decision-Making

NBS - Nature-Based-Solutions

OSM – Open Street Maps

PCA - Principal Component Analysis

SS - Silhouette Score

SUHI - Surface Heat Island

UA – Urban Atlas

UTC - Coordinated Universal Time

2. Introduction

Urban heat has become a critical challenge for cities, as rising temperatures associated with climate change intensify the frequency and severity of thermal extremes (Santamouris, 2022). A central component of this challenge is the Surface Urban Heat Island (SUHI) effect, defined as the temperature difference between urban areas and their rural surroundings. SUHI results from the combined effects of land cover, built environment, and human activities (IPCC, 2022), producing spatially uneven thermal conditions that place significant pressure on public health, energy systems, and urban infrastructure (Zhao et al., 2021; Mora et al., 2017). These conditions have increased demand for analytical tools capable of identifying where surface heat concentrates and how it relates to the physical and functional structure of the city (Melis et al., 2023).

Capturing these patterns is complex. SUHI reflects both the physical form of the city, such as building density, green cover, elevation, street configuration, as well as the social characteristics of its inhabitants, including demographic vulnerability and exposure (Gao et al., 2022). This combination makes surface heat inherently multidimensional, shaped by what are often described as formal (morphological) and functional (activity-based) determinants of urban climate (You et al., 2023). The challenge is particularly acute in dense or topographically irregular cities, where thermal variation occurs at fine spatial scales that matter for planning and design (Mansouri & Zarghami, 2025). As cities increasingly seek interventions such as Nature-based Solutions, shading strategies, or microclimatic improvements, the need for spatial representations of heat that are actionable at the scale of neighbourhoods, blocks, and specific sites becomes more pressing (Mosca et al., 2024). For planners and designers, such representations must integrate both formal and functional attributes, reflecting the way design practice interprets and transforms urban space (Kang et al., 2022). This issue appears across different ways of deriving spatial thermal information, since heat can be measured through complementary approaches such as in-situ sensor networks related to air temperature, humidity, and radiation as well as physiological indexes (Kousis et al., 2021, Ketterer & Matzarakis, 2014). Nonetheless, Earth Observations (EO) remains a widely used, pragmatic option for broad and spatial contiguous coverage of SUHI (Stewart, 2024), especially where dense ground-based measurements are unavailable, such as remote peri-urban areas. However, SUHI can oversimplify near-surface and microclimatic conditions due to it representing surface thermal conditions only and not being a direct proxy for near-surface air temperature or pedestrian-level heat exposure, which depend on additional microclimatic factors such as humidity, radiation, wind, and shading (Chakraborty et al., 2022; Briegel et al., 2025).

EO datasets from Landsat 8/9 and Sentinel 3 have been widely used to map hotspots and examine relationships between thermal behaviour, land cover, and morphology (Kim & Brown, 2021; Sidiqui et al., 2022; Assaf & Assaad, 2024). However, the way LST data are typically operationalised often introduces a structural mismatch with the spatial scales and categories used in planning and design. Classification systems such as Local Climate Zones (LCZs) offer a common language for linking morphology and climate, but their coarse typologies frequently fail to capture the microscale heterogeneity that shapes thermal behaviour in complex urban settings (Stewart, 2024). As a result, EO-based assessments, while indispensable for understanding thermal patterns, do not inherently align with the spatial logic through which planners and designers interpret, regulate, and ultimately transform urban space.

A key source of misalignment lies in the spatial units used to structure SUHI analysis. Many studies rely on administrative or statistical units, such as census blocks (Ascencio et al., 2023; Assaf & Assaad, 2024), street networks (Chen et al., 2022; Liu et al., 2024), districts (Sidiqui et al., 2022), because they facilitate demographic integration and policy reporting. However, these units are not designed to represent the built environment.

Their boundaries frequently cut across coherent morphological structures, mixing building types, densities, and land uses in ways that obscure relationships between form and thermal behaviour (Chen et al., 2023). This issue is compounded by the Modifiable Areal Unit Problem (MAUP), which can alter correlations, rankings, and hotspot identification depending on how data are aggregated (Chen et al., 2023). In practice, this means that the identification of "high risk areas" may reflect the geometry of the units rather than the underlying thermal conditions. As a result, many SUHI assessments remain difficult to translate into design relevant insights, particularly when planners and architects operate at scales that differ from those used in analysis (Keith et al., 2023).

An urban morphological perspective helps addressing these limitations. Specifically, morphometric and morphogenetic approaches generate spatial modules derived from the internal structure of the city by capturing configurational characteristics such as barriers and connectivity elements and linking them to functional and environmental data (Dibble et al., 2019; Wang et al., 2023; Arribas-Bel & Fleischmann, 2022). By grounding analysis in morphology rather than administrative boundaries, these approaches steer EO thermal assessment toward the spatial frameworks that underpin design practice and territorial governance (Chen et al., 2023).

Surface thermal risk prioritisation, limited to the assessment of EO surface conditions, is nevertheless multidimensional: hazards, exposure, and vulnerability interact across variables that differ in scale, behaviour, and epistemic status. Multicriteria Decision-Making (MCDM) methods provide a structured means of synthesising such heterogeneous data, producing objective and reproducible rankings (Rahman & Pekkat, 2024). Their flexibility has made them widely used in environmental risk assessment and climate adaptation planning (Reyes-Norambuena et al., 2024). Nonetheless, MCDM outcomes remain sensitive to methodological choices as weighting schemes are often subjective, algorithmic logics can produce divergent results, and the influence of spatial units on rankings is rarely examined (Qi et al., 2023). These issues are particularly problematic for site selection, where methodological artefacts can be mistaken for territorial conditions.

Taken together, and in relation to EO data, these observations reveal three persistent gaps. First, SUHI assessments often rely on spatial units that do not correspond to how planners and designers' structure or transform urban space, limiting the interpretability of results (Chen et al., 2023; Keith et al., 2023). Second, formal and functional determinants of heat are frequently analysed separately, preventing a relational understanding of how surface-thermal hazard and broader heat-risk conditions emerge from their interaction (Gao et al., 2022; Dibble et al., 2019; Wang et al., 2023). Third, methodological choices in MCDM workflows, i.e. spatial units, weighting schemes, algorithmic logics, are rarely subjected to sensitivity analysis, making it difficult to distinguish robust territorial patterns from artefacts of the analytical process (Rahman & Pekkat, 2024; Reyes-Norambuena et al., 2024; Qi et al., 2023).

This paper responds to these challenges by proposing a framework that repositions EO-based surface thermal assessment within the relational structure of urban form and functions. It does so through three aims. The first is to define a method capable of identifying where areas prioritised in urban planning to contain and mitigate urban heat emerges by combining morphogenetic spatial modules, objective MCDM weighting, and spatially lagged clustering. The second is to examine how methodological decisions, especially the choice of spatial units, shape the identification of priority sites for climate adaptation interventions. The third is to explore how this spatially aligned data can be used to characterize and compare different sites by classifying them into homogeneous clusters. Through these aims, the paper advances a more spatially coherent and operational understanding of site selection for urban design. Its novelty lies in testing the combined use of morphogenetic spatial units, MCDM methods, objective weighting schemes, and sensitivity analysis for EO-based spatial prioritisation, with specific attention to how spatial representation and methodological choices affect the identification and characterization of priority sites.

3. Methodology

The methodology to select and characterise urban areas for SUHI mitigation is divided into six steps (Fig. 1). (1) Data selection, where we select the variables and retrieve the opensource data to run the analysis. (2) Data modelling, in which we generate the spatial modules used to model data, and compute SUHI and all other variables. (3) Spatial association, where spatial data is correlated based on the size and location of each spatial module. (4) Site selection, in which each module is ranked based on MCDM criteria and compared through sensitivity analysis. (5) Comparison, to assess the relative differences between different spatial approaches. (6) Site characterization, by creating homogeneous clusters of urban areas to assess the comparison within and between cities.

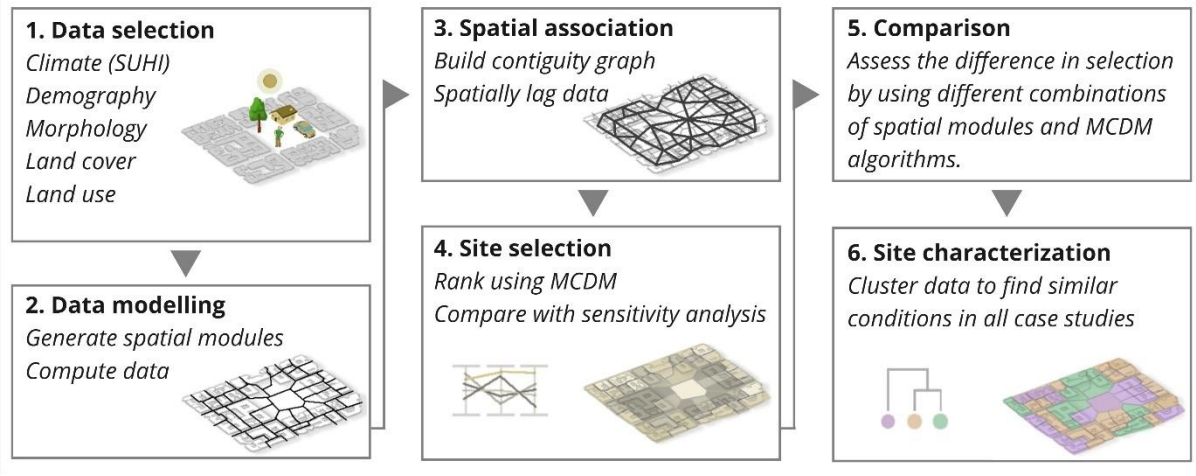


Figure 1. Six steps of the methodology.

We test the methodology developed in this study on the two Italian case studies of Genoa and Turin, chosen for their contrasting morphology and climate. Genoa, a coastal city enclosed by steep hills, has narrow urban canyons, high humidity, and 559,000 residents

over 240 km² (average 15 °C). Turin, by contrast, lies on the plain along the River Po, with a compact urban fabric, 851,000 residents over 130 km² (average of 12 °C). To ensure comparability and capture representative urban heat conditions, the analysis focuses on a period with low cloud cover, consistent acquisition times, and shared data layers. An aerial overview of the two study areas highlights these differences and provides context for interpreting the results (Fig. 2).



Figure. 2. Aerial view of the case studies: Genoa (left) and Turin (right).

3.1. Data selection

In this study, SUHI derived from EO is used as a surface-thermal hazard indicator within a broader risk prioritisation framework that combines hazard, exposure, and vulnerability variables. From the literature, we select a list of variables that are shown to influence urban inhabitants deriving from different urban dimensions such as weather and climate, demography, morphology, land cover, and land use. Doing so, we encompass different dimensions of cities that characterize urban conditions such as SUHI (Pena Acosta et al., 2023), for a total of 54 variables fully listed in the supplementary materials (Annex A).

3.2. Data modelling

3.2.1. Generating the spatial modules

We use two spatial modules in the analysis to be able to compare the effectiveness and weight of each in selecting and characterizing urban areas for SUHI risk. We select Enclosed Tessellations (ET) as the morphometric spatial module, and Census Blocks (CB) as a more traditional spatial module.

ET are defined as a set of closed contiguous polygons built from bi-dimensional morphological features (Fleischmann et al., 2021). These features are selected from built environments traits and commonly regarded as physical barriers to humans. Additional details can be found in the supplementary material (Annex A).

We used CB from the Italian cadastre database from 2011, that are compatible with the most recent census data from 2021 (ISTAT, 2021).

3.2.2. Compute SUHI from EO data

SUHI intensity was assessed for Genoa and Turin during the anomalously hot summer of 2022 (NOAA, 2023), using Landsat 8–9 imagery acquired between 1 July and 15 August. Landsat data were preferred over coarser-resolution missions (e.g., Sentinel-3) because of their finer spatial resolution and effective revisit time of less than 8 days under clear-sky conditions, when acquisitions from different orbital paths are considered. The Landsat Collection 2 Level 2 Surface Temperature product is distributed at 30 m pixel size, although the TIRS thermal bands have a native Ground Sampling Distance (GSD) of 100 m. This distinction between native sensor sampling and product pixel size is relevant when interpreting the effective spatial detail of satellite-derived thermal information (Cenci et al., 2021). Only daytime acquisitions were used, with local times between approximately 10:0 and 10:18 UTC (12:05–12:18 CEST), excluding images with high cloud cover over the study areas. These observations capture surface thermal conditions at satellite overpass time rather than the full diurnal cycle (which may exclude potential heat peaks), yet they provide spatially continuous and consistent information on intra-urban thermal patterns and hotspots. Within this study, they serve as the thermal component of the assessment and should not be interpreted as representative of overall urban heat risk, nor proxies of other heat indicators such as near-surface air temperature or pedestrian-level heat stress, which depend on additional atmospheric and microclimatic factors (Chakraborty et al., 2022; Briegel et al., 2025).

Data pre-processing involved masking residual clouds, cloud shadows, and poor-quality pixels using the QA_PIXEL band. Each scene was subsetted to an Area of Interest (AOI), defined by the municipal boundaries of each city extended with a buffer derived from the Global Human Settlement – Functional Urban Areas (GHS-FUA) layer (Schiavina et al., 2023), to include commuting zones. LST values were then converted to Celsius, stacked for each AOI, and used to compute the pixel-wise 50th percentile (50p), producing a representative LST map for summer 2022.

SUHI characterization followed the “buffer area around the city” method (Raj & Yun, 2023). In every AOI, urban and rural pixels were distinguished using Corine Land Cover 2018 Level 1 classes: “Artificial Surfaces” were classified as urban, while “Agricultural” and “Forest/seminatural” were considered rural; “Wetlands” and “Water Bodies” were excluded. To do so, the Corine raster (pixel size: 100 m) was resampled and reprojected to the Landsat grid. Finally, for every 50p LST map of each city, SUHI intensity was calculated by subtracting the mean LST value of the AOI rural pixels from every urban (and non-urban) pixel located inside the municipal boundaries. Pixels outside administrative boundaries were masked to highlight the urban–rural thermal contrast in the city area.

3.2.3. Compute all other variables

We developed fully automatic pipelines to download and model all variables but SUHI. Wind speed data, EO-composite demographic data, elevation data, building height data,

land covers are loaded as rasters, and zonal statistics is run to extract mean and standard deviation. Built-up area is analysed with zonal statistics but is averaged from Open Street Maps (OSM) building data used for ET construction and Urban Atlas (UA) data for building height. Direct demographic data comes from Italian cadastre and is extracted from the original CB and resampled. Finally, land use data is expressed in term of distances. Spatial data is selected from OSM with specific tags, and UA, and distances from the centroids are defined using a K-Neighbours Tree. Further details are found in the supplementary data as commented Jupyter notebooks.

3.3. Spatial association

We use spatial association to reinforce the morphological connection of urban data by introducing mathematical relationships in the dataset referred to the dimensions and vicinity of all polygons. This step is significant in highlighting differences between different spatial patterns, confronting both geometric entities and data attributes (Long & Robertson, 2018). We add spatial weights to each polygon based on contiguity, meaning the vicinity between each polygon and its neighbours. We calculate the queen contiguity weight matrix based on the polygons' centroids. We consider queen contiguity a suitable spatial weight for our application since the phenomenon is analysed at scales relevant for urban regulation and building-scale planning.

3.4. Site selection

The site selection process is based on the output of TOPSIS and VIKOR algorithms, comparing two different algorithms to assess the differences in terms of spatial prioritisation, i.e. "risk" in the context of the application (Kizielewicz et al., 2023). TOPSIS ranks alternatives based on their closeness to the ideal solution and distance from the worst solution. VIKOR instead focuses on identifying a compromise solution that is closest to the ideal by adhering to acceptable advantage to the optimization stability conditions. Due to the algorithms' requirements, weights were determined using different objective methods in the entropy and the Gini methods. The entropy method measures the importance of criteria based on their variability or uncertainty in the data, while the Gini method assesses criteria importance by analysing the inequality or dispersion of values. The usage of objective weighting criteria lowers the effect of redundancy in optimization criteria due to collinearity, rescaling the individual weights for those criteria that are known to be dependent (e.g., Citizen with low or no education and Citizen with degrees). Redundancy was examined post hoc using Pearson's ρ to understand how dependent variables behaved within the weighted decision matrix. We use pymcdm implementations of TOPSIS, VIKOR, and the different weights (Kizielewicz et al., 2023).

We extract from our original variable matrix those variables for which a monotonic direction of influence over SUHI can be reasonably specified, i.e. that can be assigned a positive or negative optimization criterion compatibly with the MCDM implementation (Table 2). TOPSIS and VIKOR require each criterio to be assigned a consistend

benefit/cost direction in term of linear scoring (coefficients in the range [–1, 1]). We therefore retain variables for which this assumption can be justified for spatial prioritisation, while acknowledging that some relationships may remain context-dependent or non-monotonic (e.g. Building Height can act either as benefit or a cost). The sensitivy analysis is used to assess the stability of rankings. In terms of internal consistency, we value retained variables that exhibit coherent behaviour across weighting schemes and algorithms.

To assess how the different spatial modules fare in identifying risk, we run a sensitivity analysis based on calculating and comparing the standard deviation of the score produced by the various methods (Stević et al., 2022) and deduce the difference in rankings based on Kernel Density Distribution by plotting pairwise plots with different weights. From this, we select the most performing weighting criteria by looking at stability and overall performance between the cases, ultimately basing the site selection.

Table 2. Subset of variables for MCDM, corresponding to the decision matrix and criterion types, divided between benefits (exacerbate SUHI risk) and costs (limit SUHI risk).

Optimization criteria	Risk components	Criterion type	Reasoning
Mean 50 percentile SUHI	Hazard	Benefit	The warmer the area, the higher SUHI (Hou et al., 2023).
Mean wind speed at 10/50/100/150/200 meters	Hazard	Cost	Strong ventilation can dissipate surface heat (Hou et al., 2023).
Mean vulnerable young citizen (0-5), indirect source	Vulnerability	Benefit	Presence of vulnerable stakeholders adds to the risk (Szagri et al., 2023).
Mean vulnerable elderly citizen (65+), indirect source	Vulnerability	Benefit	
Mean population density, indirect source	Vulnerability	Benefit	
Mean vulnerable young citizen (0-5), direct source	Vulnerability	Benefit	
Mean vulnerable elderly citizen (65+), direct source	Vulnerability	Benefit	
Citizen with low or no education	Vulnerability	Benefit	Vulnerable citizen that may be less receptive to risk mitigation strategies (such as
Citizen from Extra EU counties	Vulnerability	Benefit	

Citizen living alone	Vulnerability	Benefit	public alarms, emergency drills and evacuations, acceptance to mitigation strategies) (Szagri et al., 2023).
Citizen with degrees	Vulnerability	Cost	Citizen that may be more receptive to risk mitigation strategies (Szagri et al., 2023).
Citizen employed	Vulnerability	Cost	
Mean elevation	Exposure	Cost	High elevation typically features lesser temperatures (Hou et a., 2023).
Mean slope	Exposure	Cost	Rugged terrain features can impede ventilation and non-uniformly exposure to heat (Hou et al., 2023).
Mean roughness	Exposure	Cost	
Mean rugosity	Exposure	Cost	
Mean building height	Exposure	Benefit	Often considered as proxy for SUHI exposure (Chen et al., 2023).
Average built up ratio	Exposure	Benefit	
Mean impervious density	Exposure	Benefit	
Mean tree cover density	Exposure	Cost	Green features lower SUHI (Eggermont et al., 2015).
Mean ratio of shrublands	Exposure	Cost	
Mean ratio of grasslands	Exposure	Cost	
Distance from transports	Vulnerability	Cost	Access points to public and private transport networks enable more connectivity and lessen isolation for stakeholders (Chen et al., 2023).
Distance from public services	Vulnerability	Benefit	Risk rises with increasing distance to and from public services (schools, town halls) and emergency facilities (hospitals, clinics) (Szagri et al., 2023).
Distance from emergency facilities	Vulnerability	Benefit	

Distance from green amenities	Vulnerability	Benefit	Close distance with parks and urban greenery lowers SUHI risk (Chen et al., 2023).
Distance from non-green amenities	Vulnerability	Cost	Grey amenities (e.g., shopping malls, luna parks) are often impervious surfaces with high stakeholder density, thus increasing SUHI (Chen et al., 2023).

3.5. Comparison between spatial modules and MCDM algorithms

We compare ET and CB by sampling a random set of 1000 shared points extracted from the case studies. From this sampled data, we study the difference in score for each MCDM algorithm and quantify the association. We display the difference through kernel distribution for each combination to represent the overall behaviour.

Additionally, we assess the stability of results across case studies by comparing ET and CB preferences for all MCDM algorithm combinations. By plotting algorithm preferences at each sample location, we can objectively identify which urban areas are more frequently classified as at-risk by specific methods. This analysis reveals where and to what extent ET and CB produce similar rankings, offering insights into the consistency of risk identification. We then run correlation analysis to quantify how each variable influences risk.

3.6. Site characterization

We characterize urban sites by grouping areas with similar features to find site conditions that are comparable. We divide risk in equal quartiles, focusing on the highest and cluster all spatially lagged variables to generate urban typologies

We reduce collinearity and simplify the features to clusters by using Principal Component Analysis (PCA), setting the number of principal components as the minimum number of eigenvalues necessary to explain 0.95 of the total variance. Then, we use Hierarchical Agglomerative Clustering (HAC), fitting the unsupervised model on the PCA reduced variables. We use sklearn implementation of PCA and HAC (Pedregosa et al., 2011). We compute HAC within a reasonably large number of classes k in the range of 2-30, selecting the best k by using the Silhouette Score and visually by plotting a clustergram, showing the closeness of the PCA weighted mean of the clusters. To study each cluster's content, we observe the mean, standard deviation and Pearson's ρ for each variable.

4. Results and Discussion

4.1. Site selection outputs

We extracted all data for Genoa and Turin, producing the ET for both Genoa and Turin, with 33052 and 20449 polygons respectively of varying sizes. CB in the same cities amounted to 3680 and 3976.

Spatial weights analysis revealed significant associations between all polygons, forming the basis for the MCDM steps. MCDM analysis generated site preferences and rankings for TOPSIS and VIKOR, using entropy and Gini weighting criteria, applied to ET and CB (Fig. 3). Four main observations emerged, including a sensitivity analysis of MCDM scores and rankings that informed the weighting criteria, and overall comparisons between methods. The resulting scores highlight the highest-priority sites for intervention in both case studies, constituting the site selection for subsequent stages.

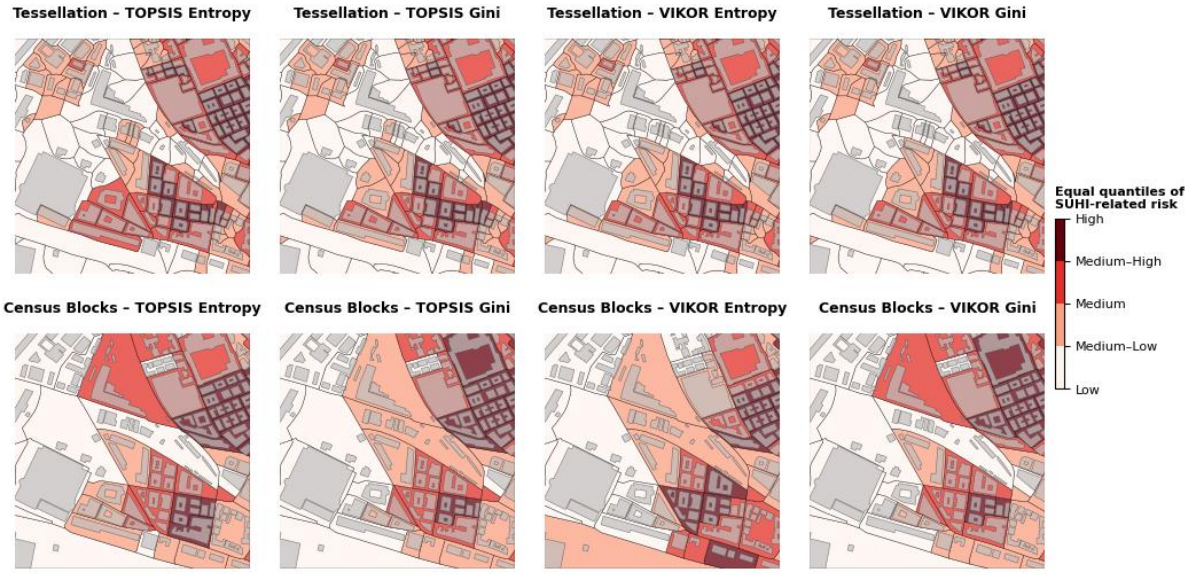


Figure 3. Excerpts from Genoa (Cornigliano) site selection process, including all possible combinations of spatial modules, MCDM, and weights.

4.1.1. Sensitivity analysis on MCDM algorithms and weights

We calculate the difference of the standard deviation of the scores, we note that location, spatial module, and MCDM algorithm each influences the variation by similar margins (Table 3). We observe that the similarity between the standard deviation of MCDM preferences was always above 83%, with the minimum value in Genoa using VIKOR with CB (83.5%), the highest in Genoa using TOPSIS (99.7%), and the mean above 91% (95.2% with TOPSIS combinations and 91.1% with VIKOR). TOPSIS favours more similar results as indicated by the lower standard deviations in all combinations and the higher standard deviation similarity between the different weights. Individual weighting methodologies did not unequivocally favour a combination of location, spatial module and algorithm. Nevertheless, the respective difference between the lowest and second lowest mean value of standard deviations for TOPSIS (entropy method) and the lowest mean value for VIKOR (Gini method) is both under 0.02, and we deem it not significant. While the

sensitivity analysis explains the stability of the approaches, with TOPSIS being generally more stable in Genoa and VIKOR in Turin, it gives insufficient insights into which approach is best.

Table 3. Standard deviation of scores (algorithm preferences) for sensitivity analysis, run by changing the weighting criteria between the different MCDM algorithms, spatial modules, and locations.

Location, Spatial module	TOPSIS scores entropy std	TOPSIS scores Gini std	TOPSIS scores std similarity [%]	VIKOR scores entropy std	VIKOR scores Gini std	VIKOR scores std similarity [%]
Genoa, ET	0.0488	0.0489	99.7428	0.1287	0.1449	88.8330
Genoa, CB	0.0563	0.0555	98.6994	0.1076	0.0898	83.4837
Turin, ET	0.0435	0.0498	87.3403	0.1303	0.1328	98.1205
Turin, CB	0.0398	0.0419	94.9958	0.0978	0.0921	94.1441
Mean	0.0471	0.0490	95.1946	0.1161	0.1149	91.1453

As a second observation, we analyse the difference in the ranking distributions (Fig. 4). In all cases, we identify the presence of two mayor poles around the lowest and highest difference in weighting criteria. These two poles correspond to urban areas that are ranked very high or very low by both algorithm combinations, meaning that all combinations rank similarly the best and worst urban areas, albeit with differences. We noted that the difference when using ET where generally smaller than CB due to the smaller spread. Notably, ET polygons are more than thrice the number of CB polygons. Thus, even if the number of features (polygons) are higher, ET shows a lower difference in ranking by changing algorithms and weighting criteria. Also, in both ET and CB case, entropy weight reduces ranking differences in confront with VIKOR. Therefore, together with the previous standard deviations analysis on scores, we selected the entropy method as our objective MCDM weighting of choice due to its better stability.

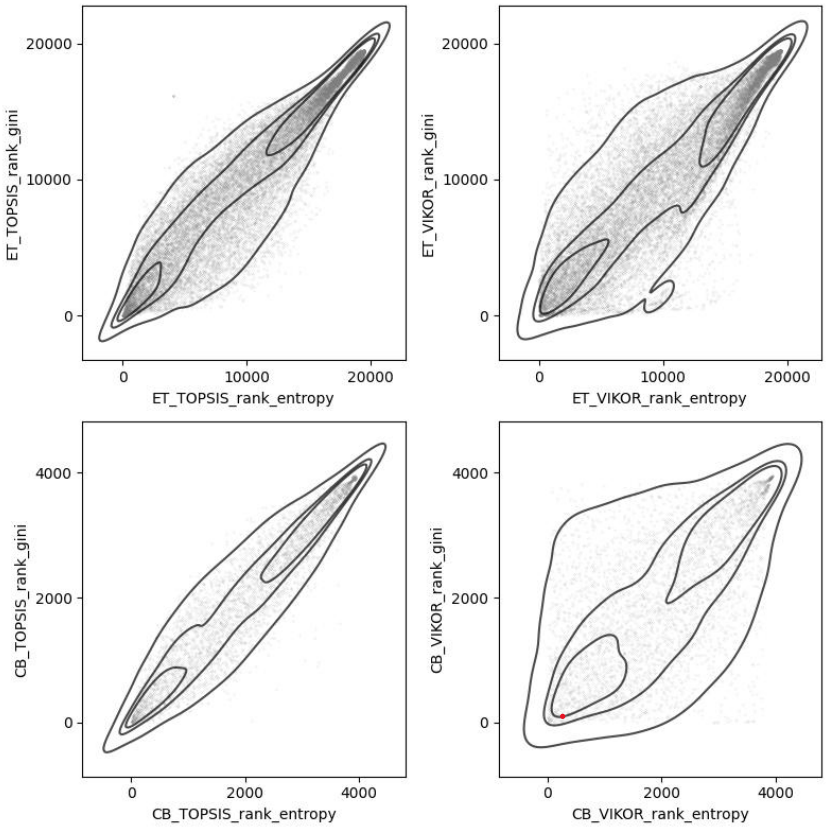


Figure 4. Pairwise plots of rankings for sensitivity analysis for the combined locations (Genoa and Turin), between the combinations of weighting criteria between the different MCDM algorithms and spatial modules (ET and CB). A superimposed Kernel Density Estimation of four levels identifies the poles.

4.1.2. Comparisons between spatial modules and MCDM algorithms

In the comparison with random samples, each optimization algorithm behaved consistently with both spatial modules (Fig. 5). This result is compatible with the previous observations. Nevertheless, for both cities VIKOR expressed preference with higher scores than TOPSIS, with a more defined prevalence for Genoa. Since we observed that TOPSIS and VIKOR ranked similarly, the difference in preference score is subjective within each algorithm. Therefore, even if VIKOR generally scored higher than TOPSIS, VIKOR defined areas are not more subjected to risk than areas defined by TOPSIS. VIKOR produced higher preference scores than TOPSIS, reflecting its tendency to assign greater values to sites representing balanced trade-offs among criteria, whereas TOPSIS scores remained lower when no site met all criteria. This is especially evident from the fact that in no case TOPSIS score is higher than 0.7, where 1 is the ideal case where all criteria would be met.

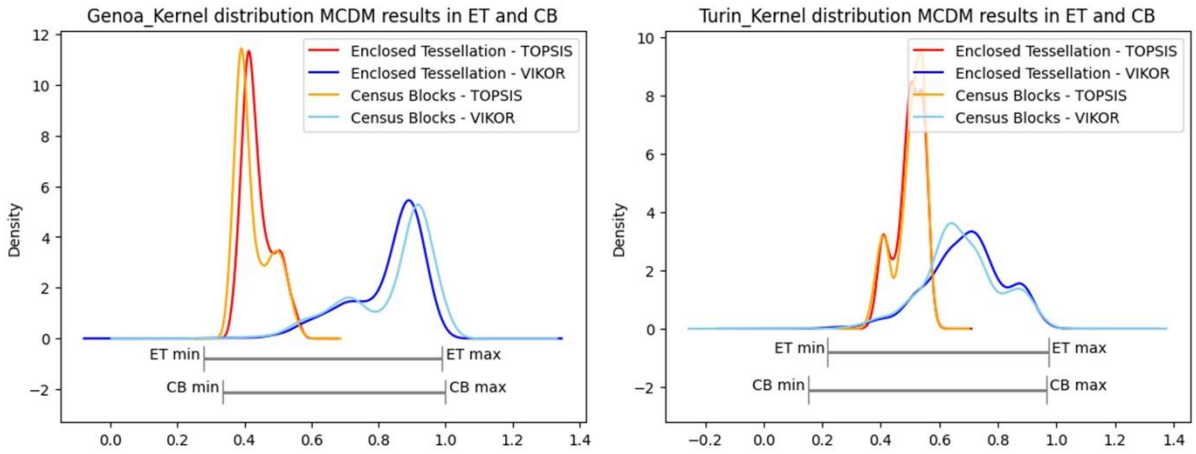


Figure 5. Kernel distribution for MCDM scores in Genoa (left) and Turin (right). Each combination of spatial module (ET and CB) and algorithm (TOPSIS and VIKOR) is considered, while highlighting the maximum and minimum values for consideration.

Finally, we deduce the difference in algorithm preference spatially in urban locations within the same set of sampled points (Fig. 6). The analysis shows that TOPSIS produces very small differences within each city, while differences are much more notable with VIKOR. This means that the score comparison in ET and CB is more similar through TOPSIS independently from the geometric attributes of each spatial modules, even in cities with significant morphological differences. VIKOR, instead, denote a higher dependence from the different geometric attributes of ET and CB, and lesser stability between the different cities. While this result is consistent with previous observations, it enables to discuss the usage of TOPSIS and VIKOR in relation to particular urban areas. Particularly, we noted that VIKOR can be more stable in representing the phenomenon in Turin, but from difference distribution we observe that the prediction can be inconsistent in regard to different neighbours.

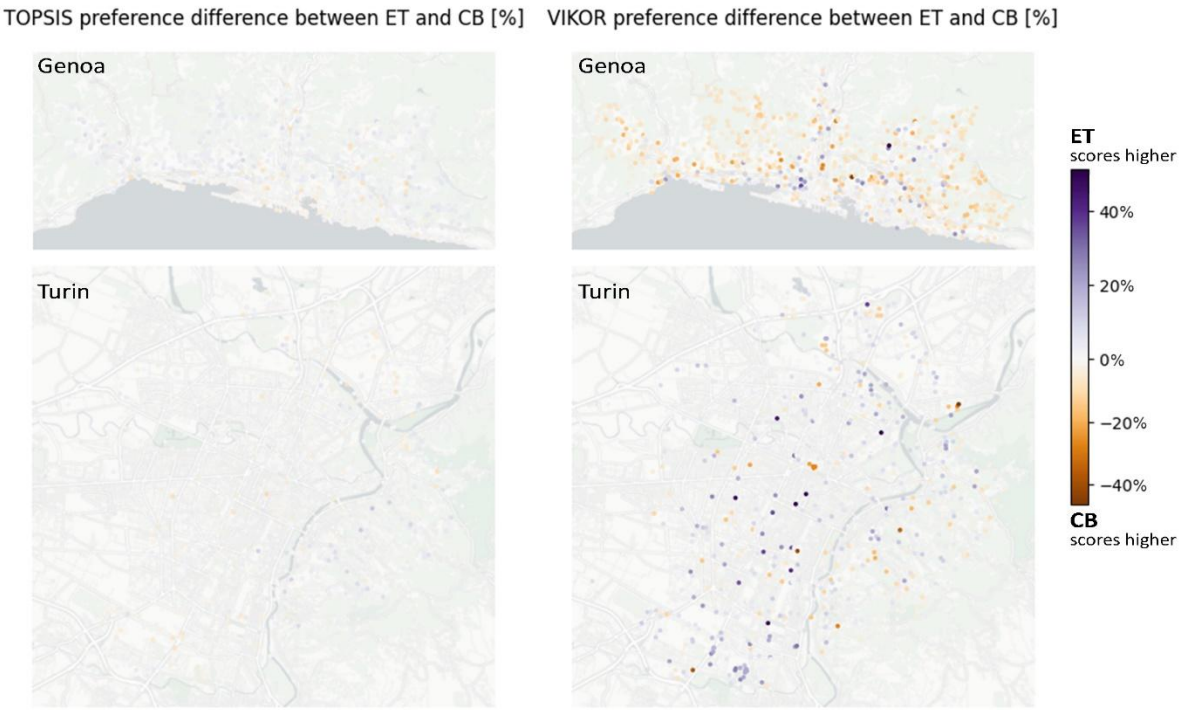


Figure 6. Spatial comparison between TOPSIS and VIKOR in Genoa (top) and Turin (bottom). TOPSIS (left) notably reduces the difference between the two spatial modules, while VIKOR (right) is more prone to prefer one spatial module to the other between different urban areas.

4.1.3. Exemplification of the site selection process

We exemplify the site selection process based on the results from the previous analysis, selecting the combination of ET with TOPSIS and entropy weights and map the scores for both Genoa (Fig. 7) and Turin (Fig. 8). The effect that each risk component has on the combined score is visually apparent and can be referred to specific variables by studying correlation.

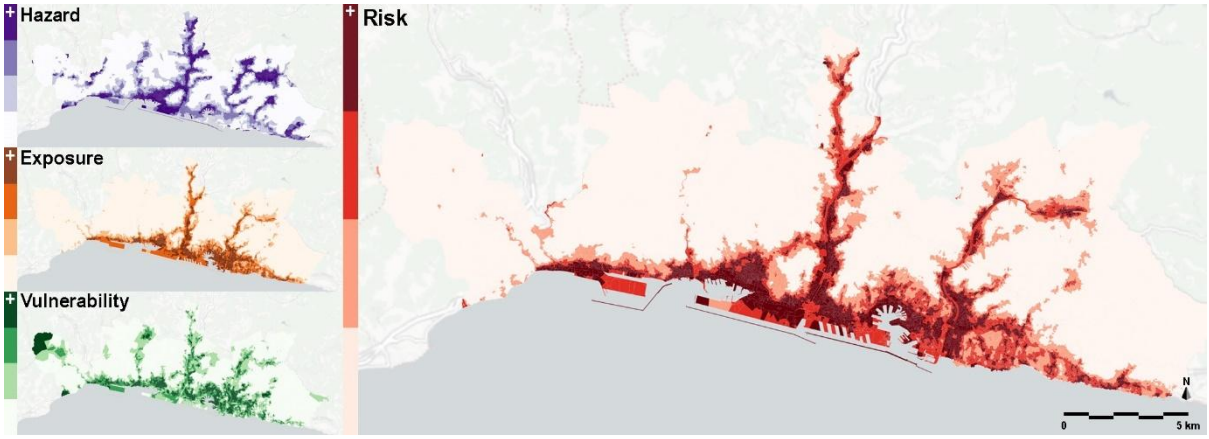


Figure 7. Spatial prioritisation of SUHI-related hazard, exposure, and vulnerability conditions, assessment for Genoa, with decomposed maps separately presenting the hazard, exposure, and vulnerability components obtained with the same combination of ET, TOPSIS, entropy weights.

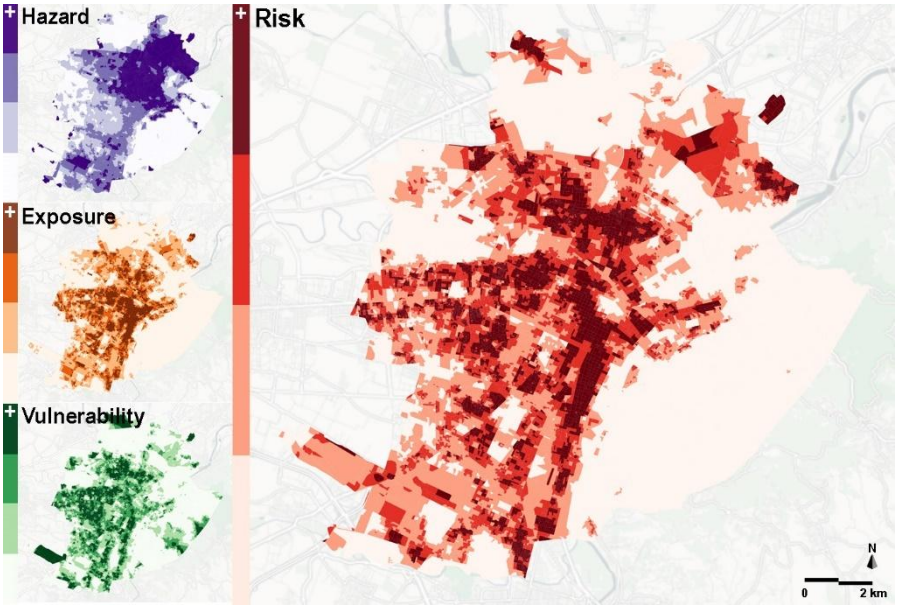


Figure 8. Spatial prioritisation of SUHI-related hazard, exposure, and vulnerability conditions, assessment for Turin, with decomposed maps separately presenting the hazard, exposure, and vulnerability components obtained with the same combination of ET, TOPSIS, entropy weights.

We analyse correlation between the composite prioritisation score, its components, and highly correlated variables using Pearson's ρ (Fig. 9). The full correlation analysis is in the supplementary material (Annex B). The matrices reveal coherent blocks of highly correlated variables (e.g., slope/roughness/rugosity; tree cover/shrubs; wind-speed layers; imperviousness/built-up ratio/SUHI). These redundancy patterns indicate that some dimensions, particularly morphology, vegetation, and built form, may receive greater implicit representation in the composite index. Although the sensitivity analysis suggests that the broad spatial prioritisation patterns remain relatively stable, the influence of correlated criteria should be considered when interpreting individual variable correlation contribution.

Within the structure of the composite index, exposure shows the strongest association with the resulting prioritisation score in both Genoa and Turin (ρ=+0.96). This should not be interpreted as independent empirical evidence that exposure is the dominant determinant of real-world heat risk, because the association partly reflects the variables and weighting structure used to construct the index. Hazard and vulnerability are also associated with the composite score, while SUHI shows high positive correlations (ρ=+0.80 in Genoa and +0.83 in Turin). Morphological characteristics, including elevation, slope, and terrain roughness, are negatively associated with the prioritisation score, particularly in Turin, and vegetation coverage shows a similar inverse relationship. These patterns are consistent with relationships reported for densely built cities (Gao et al., 2022), but they should be interpreted as characteristics of the prioritisation model rather than as independently validated causal effects.

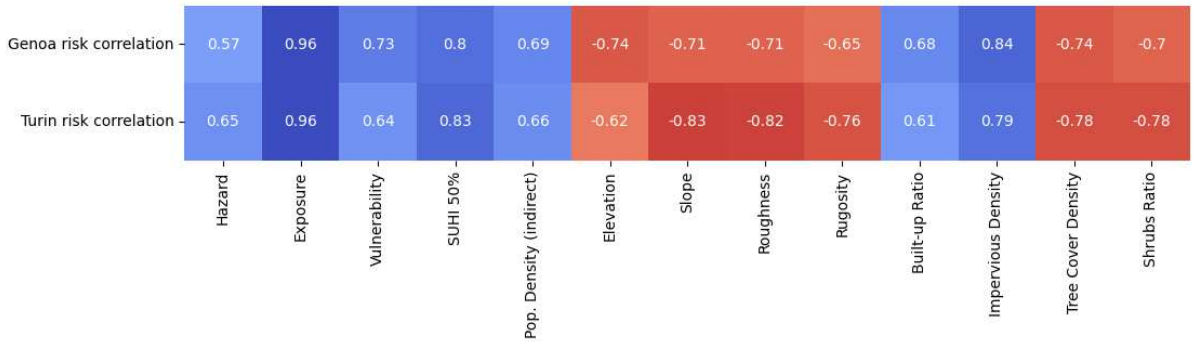


Figure 9. Pearson's ρ correlation analysis of risk in Genoa and Turin with risk components and highly correlated variables (|ρ|≥+0.6).

4.1.4. Comparison with existing studies

In Genoa and Turin, our spatial-MCDM framework indicates that SUHI risk is most pronounced in areas with limited vegetation, dense urbanization, and socio-economic vulnerability. Nonetheless, computed SUHI risk represents a conceptual form of risk rather that a true predictor in absence of similar resolution data on city-level health or damage. Focusing on risk as a spatial prioritization tool, similar patterns have been reported elsewhere: Morabito et al. (2015) mapped elderly heat risk in Italian cities and showed that vulnerability factors can outweigh temperature extremes, while Pappalardo et al. (2023) highlighted how socio-demographic disadvantage shapes risk distribution in Padua from a climate-justice perspective. In Genoa, Morabito explicitly identified Cornigliano (an industrial and densely built district with limited green space) as the highest-risk area, and our analysis confirmed that this neighbourhood remains a critical hotspot. For Turin, Morabito's maps pointed to elevated risk in the central urban districts, where high surface temperatures overlap with a dense elderly population; our results found similar patterns. Additionally, our sensitivity analysis found that entropy weight with TOPSIS provided clear discrimination, whereas VIKOR produced more stable rankings in Turin. These differences echo earlier approaches: Morabito et al. used statistical downscaling to refine LST estimates, while Pappalardo et al. applied composite GIS indices to capture equity concerns. Public-health studies further support the need for validation. For example, Ghirardi et al. (2015) linked heat waves to emergency visits across age groups, and Cremonini & Georgiadis (2025) stressed elderly vulnerability under climate change.

Although these comparisons provide only an approximate external reference and cannot fully validate the framework (especially in relation to compound risk), they help situate the results within known territorial patterns, as the methodology is intended as a spatial prioritisation tool rather than a predictor of human impact. Comparisons suggest that our framework is consistent with existing evidence but would benefit from further testing against health outcomes and broader adaptation strategies.

Additionally, for practical use by planners, results must be screened against regulations that may restrict interventions, e.g. conservation policies in historic centres, or physical

constraints such as street geometry (Privitera & Jelo, 2025). The system allows such filters to be added either as masking layers or as variables before MCDM ranking. Operationally, the workflow provides two complementary outputs: a ranked set of spatial units indicating where intervention may be prioritised, and a multivariate description of the conditions characterising each priority site. These outputs do not prescribe a design solution; rather, they provide a spatially explicit basis for subsequent feasibility screening, intervention selection, and site-specific design analysis.

4.2. Site characterisation

We group data from Genoa and Turin with the highest quartile risk scores set in the site selection step. PCA reduced the features from 57 to 17 and clustered with HAC by choosing the best class number k=8 judging from the Silhouette Score (SS=0.176) and visually from the clustergram (Annex C). Clustering separation, even on the best k, is modest, indicating that the typologies should be interpreted as integrative descriptors rather than generalised design rules. On one hand, this is expected due to the diversity of the case studies. On the other hand, the present application is necessarily limited in scope, and the inclusion of additional cities would help strengthen cluster robustness and broaden the operational relevance of the typologies.

We extracted each cluster's content from the spatially lagged variables and analysed them in the supplementary material (Annex D). The resulting cluster represent distinct typologies of high-risk urban areas, each defined by a unique combination of climate, demography, morphology, land cover, and land use characteristic. We obtained six clusters in Genoa (Fig. 10) and three in Turin (Fig. 11).

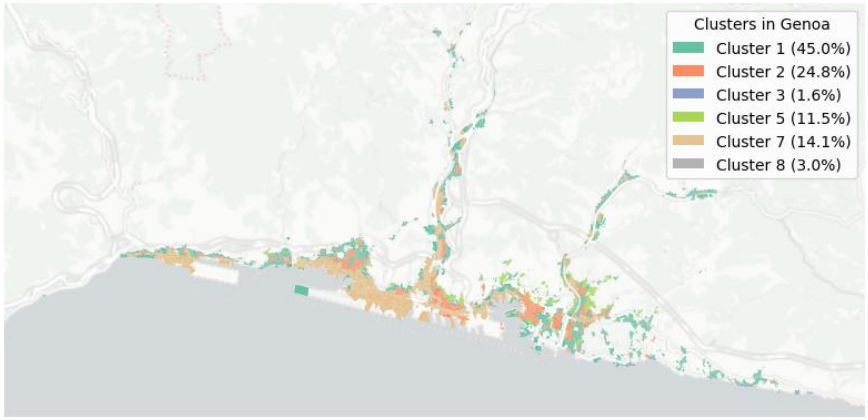


Figure 10. Site characterization by clustering the highest quartile of areas under SUHI risk in Genoa, grouping areas with similar profiles in terms of climate, demography, morphology, land cover, and land use. Percentages show the occurrences of each cluster in Genoa.

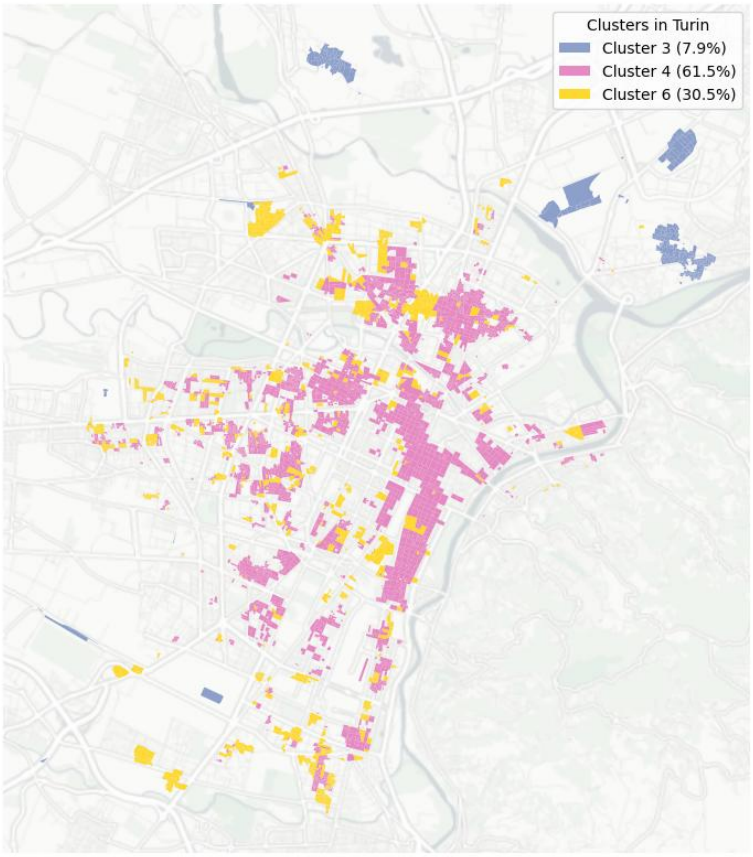


Figure 11. Site characterization by clustering the highest quartile of areas under SUHI risk in Turin, grouping areas with similar profiles in terms of climate, demography, morphology, land cover, and land use. Percentages show the occurrences of each cluster in Turin.

From this we can derive some findings on the characterization of each cities' most risk-prone areas. The first finding regards the overall relative characteristics of each city. Turin is simpler with only three different clusters of risk-areas, while Genoa is more complex having six clusters. Additionally, both cities present a non-uniform subdivision of areas between the different clusters, meaning that some urban typologies under high-risk already hold a predominant presence in the city (Cluster 1, 45.0% in Genoa; Cluster 4, 61.5% in Turin).

Secondly, the between-cities comparison is greatly limited, being characterised by a sole cluster found in both cities (Cluster 3, 1.6% of Genoa and 7.9% of Turin, in total 4% of all data). This result, while expected due to the differing morphology between Genoa and Turin, nevertheless highlights some areas that share similar features. Specifically, these are characterized by high variability due to SUHI, demography, imperviousness, and land use, while having low variability in building height. Generally, these areas are found away from the city centres, along the seaside in Genoa and in peri-urban areas in Turin.

Site characterization complements the selection by linking heat prioritisation to urban typologies, enabling immediate description of local conditions and their relation to

surrounding areas. This supports multi-scalar approaches for planning and forecasting Nature-Based-Solutions (NBS) performance, which depends heavily on accurate site conditions (UNDRR & UNU-EHS, 2023). For example, urban canyons, defined as the cross-section of two buildings and the street between and commonly used in urban design for thermal regulation (Mosca et al., 2024), can be retrieved from ET modules and connectivity graphs, allowing detailed analysis of canyon morphology within the same framework.

5. Conclusions

This study developed a spatial method that weighs different form-based modules to support EO-based heat adaptation planning through site selection and site characterisation. The approach aligns spatial prioritisation with how planners and architects read urban space, linking surface heat to familiar urban forms and functions.

Across Genoa and Turin, vegetation cover, built-up density, and demographic indicators emerged as the most influential drivers of SUHI and associated heat-risk conditions. Comparing spatial modules, MCDM algorithms, and weighting criteria showed that different configurations lead to different planning insights. Enclosed Tessellation combined with TOPSIS produced the clearest and most stable site-selection results, while the framework remains flexible enough to adapt to different planning objectives.

Clustering supports planning by characterizing urban sites, distinguishing local urban forms and functional conditions with similar patterns. This approach revealed descriptive clusters of high-priority areas high-risk clusters within each city, allowing for comparisons across recurring combinations of urban characteristics rather than isolated locations. The limited number of case studies ultimately limits the generalisation of the found typologies, and a higher city count could improve on the robustness of typology workflow.

The workflow is automated and reproducible, and can handle heterogeneous datasets, but its scope is constrained by several factors. The primary limitation of the study is the low number of case studies, selected in part to simplify LST image acquisition and processing. While sufficient to test the framework, this limits generalisation: the “best performing” combination of spatial modules and MCDM algorithms may differ in other urban contexts. Although TOPSIS appeared more stable than VIKOR in our setting, wider application is needed to confirm this, and additional site-characterisation clusters are likely to emerge as more cities are included. Further research will focus on expanding the case studies to different cities, exploring how similar spatial sensitivity behaves in different urban contexts. Additionally, application of both site selection and characterization methods will be applied to street-level applications, such as in supporting the locating and designing of climate-adaptation interventions. Finally, we envision that morphological approaches that focuses on form and function could be similarly constructed by using different dataset on hazard (such as air temperature, but also related to different hazards such as flooding or biodiversity loss), expanding on the

556 correlation between risk assessment and the MAUP problem that strongly influence how
557 designers and urban planners transform and adapt cities.

558 ## 6. References

559 Assaf, G., & Assaad, R. H. (2024). Using Data-Driven Feature Engineering Algorithms to
560 Determine the Most Critical Factors Contributing to the Urban Heat Island Effect
561 Associated with Global Warming. 1055–1062.
562 https://doi.org/10.1061/9780784485248.126

563 Briegel, F., Pinto, J. G., & Christen, A. (2025). Is satellite land surface temperature an
564 appropriate proxy for intra-urban variability of daytime heat stress? Remote Sensing of
565 Environment, 315, 115045. https://doi.org/10.1016/j.rse.2025.115045

566 Cenci, L., Pampanoni, V., Laneve, G., Santella, C., & Boccia, V. (2021). Presenting a Semi-
567 Automatic, Statistically-Based Approach to Assess the Sharpness Level of Optical Images
568 from Natural Targets via the Edge Method. Case Study: The Landsat 8 OLI–L1T Data.
569 Remote Sensing, 13(8), 1593. https://doi.org/10.3390/rs13081593

570 Chakraborty, T., Venter, Z. S., Qian, Y., & Lee, X. (2022). Lower urban humidity
571 moderates outdoor heat stress. *AGU Advances*, 3,
572 e2022AV000729. https://doi.org/10.1029/2022AV000729

573 Chen, TH.K., Prishchepov, A.V., Sabel, C.E. (2023). Detecting Urban form Using Remote
574 Sensing: Spatiotemporal Research Gaps for Sustainable Environment and Human
575 Health. In: Wen, TH., Chuang, TW., Tipayamongkholgul, M. (eds) Earth Data Analytics for
576 Planetary Health. Atmosphere, Earth, Ocean & Space. Springer, Singapore.
577 https://doi.org/10.1007/978-981-19-8765-6_10

578 Chen, Y., Shan, B., & Yu, X. (2022). Study on the spatial heterogeneity of urban heat
579 islands and influencing factors. *Building and Environment*, *208*, 108604.
580 https://doi.org/10.1016/j.buildenv.2021.108604

581 Cremonini, L., & Georgiadis, T. (2025). Urban effects of climate change on elderly
582 population and the need for implementing urban policies. *Encyclopedia, 5*(3), 140.
583 https://doi.org/10.3390/encyclopedia5030140

584 Dibble, J., Prelorendjos, A., Romice, O., Zanella, M., Strano, E., Pagel, M., & Porta, S.
585 (2019). On the origin of spaces: Morphometric foundations of urban form evolution.
586 *Environment and Planning B: Urban Analytics and City Science*, *46*(4), 707–730.
587 https://doi.org/10.1177/2399808317725075

588 Fleischmann, M., Romice, O., Porta, S., 2021. Measuring urban form: Overcoming
589 terminological inconsistencies for a quantitative and comprehensive morphologic
590 analysis of cities. Environment and Planning B: Urban Analytics and City Science 48,
591 2133–2150. https://doi.org/10.1177/2399808320910444

592 Gao, Y., Zhao, J., & Han, L. (2022). Exploring the spatial heterogeneity of urban heat
593 island effect and its relationship to block morphology with the geographically weighted
594 regression model. *Sustainable Cities and Society*, *76*, 103431.
595 https://doi.org/10.1016/j.scs.2021.103431

596 Ghirardi, L., Bisoffi, G., Mirandola, R., Ricci, G., & Baccini, M. (2015). The impact of heat
597 on an emergency department in Italy: Attributable visits among children, adults, and the
598 elderly during the warm season. *PLOS ONE, 10*(10), e0141054.
599 https://doi.org/10.1371/journal.pone.0141054

600 Heris, M. P., Muller, B., & Wilson, A. M. (2023). Why Does Planning Matter in
601 Microclimate Management and Urban Heat Mitigation? *Journal of Planning Education*
602 *and Research*, *43*(2), 371–387. https://doi.org/10.1177/0739456X19883000

603 Hou, H., Su, H., Yao, C., & Wang, Z (2023), Spatiotemporal patterns of the impact of
604 surface roughness and morphology on urban heat island, Sustainable Cities and Society,
605 92, 104513, https://doi.org/10.1016/j.scs.2023.104513.

606 IPCC (2022). Climate Change 2022: Impacts, Adaptation, and Vulnerability. Contribution
607 of Working Group II to the Sixth Assessment Report of the Intergovernmental Panel on
608 Climate Change [H.-O. Pörtner, D.C. Roberts, M. Tignor, E.S. Poloczanska, K. Mintenbeck,
609 A. Alegría, M. Craig, S. Langsdorf, S. Löschke, V. Möller, A. Okem, B. Rama (eds.)].
610 Cambridge University Press. Cambridge University Press, Cambridge, UK and New York,
611 NY, USA, 3056 pp., https://doi,org/10.1017/9781009325844

612 Kabisch, N., Korn, H., Stadler, J., & Bonn, A. (2017). Nature-based solutions to climate
613 change adaptation in urban areas: Linkages between science, policy and practice.
614 Springer. https://doi.org/10.1007/978-3-319-56091-5

615 Kang, S., Lee, D., Park, J., & Jung, J. (2022). *Exploring urban forms vulnerable to urban*
616 *heat islands: A multiscale analysis*. Sustainability, 14(6), 3603.
617 https://doi.org/10.3390/su14063603

618 Keith, L., Gabbe, C. J., & Schmidt, E. (2023). Urban heat governance: Examining the role
619 of urban planning. *Journal of Environmental Policy & Planning, 25*(5), 642–662.
620 https://doi.org/10.1080/1523908X.2023.2231234

621 Ketterer, C., & Matzarakis, A. (2014). *Human-biometeorological assessment of the urban*
622 *heat island in a city with complex topography: The case of Stuttgart, Germany*. Urban
623 Climate, 10(Part 3), 573–584. https://doi.org/10.1016/j.uclim.2014.01.003

624 Kim, S. W., & Brown, R. D. (2021). Urban heat island (UHI) intensity and magnitude
625 estimations: A systematic literature review. *Science of The Total Environment*, *779*,
626 146389. https://doi.org/10.1016/j.scitotenv.2021.146389

627 Kousis, I., Pigliautile, I. & Pisello, A. Intra-urban microclimate investigation in urban heat
628 island through a novel mobile monitoring system. *Sci Rep* 11, 9732 (2021).
629 https://doi.org/10.1038/s41598-021-88344-y

630 Liu, Q., Xie, M., Peng, J., Zhou, X., Yang, K., Zhu, R., & Liu, Y. (2024). *Revealing the urban*
631 *heat exposure risk network: Exploring the possibility of mitigating heat-related risks from*
632 *a network perspective.* Sustainable Cities and Society, 112, 105592.
633 https://doi.org/10.1016/j.scs.2024.105592

634 Long, J., & Robertson, C. (2018). Comparing spatial patterns. *Geography Compass*, *12*(2),
635 e12356. https://doi.org/10.1111/gec3.12356

636 Mansouri, S. T., & Zarghami, E. (2025). *Investigating the effect of the physical layout of*
637 *the architecture of high-rise buildings, residential complexes, and urban heat islands*.
638 Energy and Built Environment, 6(1), 1–17.
639 https://doi.org/10.1016/j.enbenv.2023.07.004

640 Meerow, S., & Newell, J. P. (2017). Spatial planning for multifunctional green
641 infrastructure: Growing resilience in Detroit. Landscape and Urban Planning, 159, 62–
642 75. https://doi.org/10.1016/j.landurbplan.2016.10.005

643 Melis, G., Di Gangi, E., Ellena, M., Zengarini, N., Ricciardi, G., Mercogliano, P., & Costa, G.
644 (2023). Urban Heat Island effect and social vulnerability in Turin: Prioritizing climate
645 change mitigation action with an equity perspective. *Science Talks*, 100258.
646 https://doi.org/10.1016/j.sctalk.2023.100258

647 Mora, C., Dousset, B., Caldwell, I. R., Powell, F. E., Geronimo, R. C., Bielecki, C. R., Counsell,
648 C. W. W., Dietrich, B. S., Johnston, E. T., Louis, L. V., Lucas, M. P., McKenzie, M. M., Shea, A.
649 G., Tseng, H., Giambelluca, T. W., Leon, L. R., Hawkins, E., & Trauernicht, C. (2017). Global
650 risk of deadly heat. *Nature Climate Change, 7*(7), 501–506.
651 https://doi.org/10.1038/nclimate3322

652 Morabito, M., Crisci, A., Gioli, B., Gualtieri, G., Toscano, P., Di Stefano, V., Orlandini, S., &
653 Gensini, G. F. (2015). Urban-hazard risk analysis: Mapping of heat-related risks in the
654 elderly in major Italian cities. *PLOS ONE, 10*(6), e0127277.
655 https://doi.org/10.1371/journal.pone.0127277

656 Mosca, F., Calbi, M., Roccotiello, E., & Perini, K (2025). A computational approach to
657 assess the effects of ecological building envelopes on outdoor thermal comfort,
658 Sustainable Cities and Society, 120, 106170, https://doi.org/10.1016/j.scs.2025.106170

659 National Centers for Environmental Information (NOAA) (2024). Annual 2023 Global
660 Climate Report. https://www.ncei.noaa.gov/access/monitoring/monthly-
661 report/global/202313

Pappalardo, S. E., Zanetti, C., & Todeschi, V. (2023). Mapping urban heat islands and heat-related risk during heat waves from a climate justice perspective: A case study in the municipality of Padua (Italy) for inclusive adaptation policies. *Landscape and Urban Planning, 243*, 104831. https://doi.org/10.1016/j.landurbplan.2023.104831

Patil, J., Maithani, S. & Sharma, S.K. (2025) Enhancing spatial resolution of Landsat derived land surface temperature: A novel downscaling approach using an extreme learning machine. *J Earth Syst Sci* 134, 3, https://doi.org/10.1007/s12040-024-02457-2

Pedregosa, F., Varoquaux, G., Gramfort, A., Michel, V., Thirion, B., Grisel, O., Blondel, M., Prettenhofer, P., Weiss, R., Dubourg, V., Vanderplas, J., Passos, A., Cournapeau, D., Brucher, M., Perrot, M., Duchesnay, E (2011). Journal of Machine Learning Research, 12, pp. 2825—2830. Retrieved from https://dl.acm.org/doi/10.5555/1953048.2078195

Pena Acosta, M., Dikkers, M., Vahdatikhaki, F., Santos, J., & Dorée, A. G. (2023). A comprehensive generalizability assessment of data-driven Urban Heat Island (UHI) models. *Sustainable Cities and Society*, *96*, 104701. https://doi.org/10.1016/j.scs.2023.104701

Privitera, R., & Jelo, G. (2025). Built Heritage Preservation and Climate Change Adaptation in Historic Cities: Facing Challenges Posed by Nature-Based Solutions. *Sustainability*, 17(13), 5693. https://doi.org/10.3390/su17135693

Qi, J., Ding, L., & Lim, S. (2023). *Application of a decision-making framework for multi-objective optimisation of urban heat mitigation strategies*. Urban Climate, 47, 101372. https://doi.org/10.1016/j.uclim.2022.101372

Rahman, A., & Pekkat, S. (2024). Identifying and ranking of CMIP6-global climate models for projected changes in temperature over Indian subcontinent. *Scientific Reports*, *14*(1), 3076. https://doi.org/10.1038/s41598-024-52275-1

Raj, S., & Yun, G. Y. (2023). Influence of selection of rural reference area for quantifying the surface urban heat islands intensity in major South Korean cities. *Architectural Science Review*, *67*(4), 345–356. https://doi.org/10.1080/00038628.2023.2290740

Reyes-Norambuena, P., Martinez-Torres, J., Nemati, A., Hashemkhani Zolfani, S., & Antucheviciene, J. (2024). Towards Sustainable Urban Futures: Integrating a Novel Grey Multi-Criteria Decision Making Model for Optimal Pedestrian Walkway Site Selection. *Sustainability*, *16*(11), 4437. https://doi.org/10.3390/su16114437

Santamouris, M. (2022). The Impact and Influence of Mitigation Technologies on Heat-Related Mortality in Overheated Cities. In N. Aghamohammadi & M. Santamouris (Eds.), *Urban Overheating: Heat Mitigation and the Impact on Health* (pp. 155–169). Springer Nature. https://doi.org/10.1007/978-981-19-4707-0_7

Schiavina, M., Moreno-Monroy, A., Maffenini, L., & Veneri P. (2023). GHS-FUA R2019A - GHS functional urban areas, derived from GHS-UCDB R2019A, (2015),

R2019A.European Commission, Joint Research Centre (JRC) [Dataset]
https://doi.org/10.2905/347F0337-F2DA-4592-87B3-E25975EC2C95

Sidiqui, P., Roös, P. B., Herron, M., Jones, D. S., Duncan, E., Jalali, A., Allam, Z., Roberts, B. J., Schmidt, A., Tariq, M. A. U. R., Shah, A. A., Khan, N. A., & Irshad, M. (2022). Urban Heat Island vulnerability mapping using advanced GIS data and tools. *Journal of Earth System Science*, *131*(4), 266. https://doi.org/10.1007/s12040-022-02005-w

Stević, Ž., Subotić, M., Tanackov, I., Sremac, S., Ristić, B., & Simić, S. (2022). EVALUATION OF TWO-LANE ROAD SECTIONS IN TERMS OF TRAFFIC RISK USING AN INTEGRATED MCDM MODEL. *Transport*, *37*(5), Article 5. https://doi.org/10.3846/transport.2022.18243

Stewart, I. D. (2024). Origins and Evolution of the Local Climate Zone Classification. In R. Wang, M. Cai, C. Ren, & Y. Shi (Eds.), *Local Climate Zone Application in Sustainable Urban Development: Experience from East and Southeast Asian High-Density Cities* (pp. 19–33). Springer International Publishing. https://doi.org/10.1007/978-3-031-56168-9_2

Szagri, D., Nagy, B., & Szalay, Z. (2023). How can we predict where heatwaves will have an impact? – A literature review on heat vulnerability indexes. *Urban Climate*, *52*, 101711. https://doi.org/10.1016/j.uclim.2023.101711

UNDRR and UNU-EHS (2023), Nature-based Solutions for Comprehensive Disaster and Climate Risk Management, United Nations Office for Disaster Risk Reduction. Retrieved from https://www.undrr.org/publication/nature-based-solutions-comprehensive-disaster-and-climate-risk-management

Wang, J., Fleischmann, M., Venerandi, A., Romice, O., Kuffer, M., & Porta, S. (2023). EO + Morphometrics: Understanding cities through urban morphology at large scale. *Landscape and Urban Planning*, *233*, 104691. https://doi.org/10.1016/j.landurbplan.2023.104691

Wong, N. H., Tan, C. L., Kolokotsa, D. D., & Takebayashi, H. (2021). Greenery as a mitigation and adaptation strategy to urban heat. Nature Reviews Earth & Environment, 2(3), 166–181. https://doi.org/10.1038/s43017-021-00133-5

You, M., Huang, J., & Guan, C. (2023). *Are new towns prone to urban heat island effect? Implications for planning form and function*. Sustainable Cities and Society, 99, 104939. https://doi.org/10.1016/j.scs.2023.104939

Zhao, L., Oleson, K., Bou-Zeid, E., Krayenhoff, E. S., Bray, A., Zhu, Q., Zheng, Z., Chen, C., & O'Neill, M. S. (2021). Global multi-model projections of local urban climates. *Nature Climate Change, 11*(2), 152–157. https://doi.org/10.1038/s41558-020-00958-8

Supplementary Files

This is a list of supplementary files associated with this preprint. Click to download.

- AnnexA.docx
- AnnexB.docx
- AnnexC.docx
- AnnexC.docx
- AnnexD.docx
- Coderepository.7z